# Nonrigidity of Pseudooctahedral $Re(CO)H_2L_2(NO)$ Complexes in Solution (L = Phosphorus Donor): Evidence for a Dihydride/Dihydrogen H/H Exchange Mechanism

Vladimir Bakhmutov,† Tobias Bürgi, Peter Burger, Urs Ruppli, and Heinz Berke*

*Anorganisch-chemisches Institut der Universität Zürich, Winterthurerstrasse 190, CH-8057 Zürich, Switzerland*

*Received March 22, 1994*®

The kinetics of H/H exchanges of $Re(CO)H_2L_2(NO)$ complexes (L = $PCy_3$ (**1**), $P(iPr)_3$ (**2**), $PMe_3$ (**3**), $P(OiPr)_3$ (**4**)) were determined by variable-temperature (40–90 °C) saturation transfer $^1H$ NMR experiments. From the kinetic data and MO calculations, an intramolecular dihydride/dihydrogen H/H exchange mechanism is proposed.

## Introduction

In view of the fact that the octahedral ligand environment is the most prevalent one within low-oxidation-state coordination chemistry, the portion of cases in which intramolecular ligand mobility is observed is relatively small[1]. Normally a strong ligand field causes a marked energetic preference for the octahedron, so that alternative geometries required as intermediates in positional ligand exchange processes are not easily accessible.

Specific changes in the substitution pattern of a complex can, however, lead to changes in the relative energies of geometrical isomers, and therefore, alternative arrangements may be found in closer energetic vicinity to the octahedral ligand environment. Hence, the dynamic behavior of octahedral systems could become feasible. Such processes have been put forward to occur via the trigonal-twist[2] or the bicapped-tetrahedron mechanism;[3] the latter has two subdivisions distinguished by a 90° or a 180° rotation of a tetrahedral edge. All these steps pass through a trigonal-prismatic intermediate.

In addition, there are hydride-specific topological rearrangements, which have mainly been observed in polyhydride compounds. These reactions often take advantage of the propensity of hydride ligands to combine with dihydrogen moieties,[4] thus inducing intramolecular H ligand scrambling by $H_2$ ligand formation with subsequent rotation of this moiety around the M–($H_2$) axis. Among 18-electron octahedral dihydride complexes with a $d^6$ configuration H/H exchange has been proposed to occur in $[Rh(tetraphos)H_2]^+$ compounds.[5] In $[Os(CO)(H_2)(NO)(PR_3)_2]^+$ species this type of reaction has also been observed, and a rearrangement path similar to the formation of an $H_2$ complex has been implied.[6] Within $d^8$ square-planar coordination, which is electronically related to the $d^6$ octahedron, *cis*-$PtH_2L_2$ (L = phosphorus donor) compounds were found to display positional exchange of the H ligands, presumably via involvement of a $Pt(H_2)$ intermediate.[7] *cis*-$MH_2L_4$ compounds[8a] (M = Fe, Ru; L = phosphorus donor) revealed fluxionality with intermediate formation of *trans*-dihydride isomers. The coordinative framework of the $FeH_2L_4$ compounds was described as a hydride-bicapped tetrahedron, in which the ligand mobility is achieved by the movement of a hydride ligand from one tetrahedral face to another. In the following this mechanism is referred to as the "tetrahedral jump". The octahedral *cis*-$Ru(CO)H_2(PPh_3)_3$ compound[8b] is proposed to rearrange nondissociatively via the trigonal-twist route. Related $FeH_2(P\frown P)_2$ complexes[9] have also been found to undergo H/H exchange, but the kinetic data did not allow definite mechanistic conclusions.

We have recently reported synthetic access to $Re(CO)H_2(NO)(PR_3)_2$ compounds,[10] which are isoelectronic with the Os systems mentioned before. In the course of NMR investigations of these complexes, H/H exchange of the two hydride ligands became apparent, and it is the intention of this paper to gain insight into the mechanism by NMR-based kinetic studies on the derivatives **1**–**4** and through MO calculations on these processes.

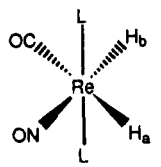


L =
$PCy_3$ **1**
$P(iPr)_3$ **2**
$PMe_3$ **3**
$P(OiPr)_3$ **4**

## Results and Discussion

**Structural Data on $Re(CO)(H)_2(NO)(PR_3)_2$ Complexes.** The X-ray crystal structure investigation of **4**[10]

† On leave from the Russian Academy of Sciences, A. N. Nesmeyanov Institute of Organo-Element Compounds, Vavilov Str. 28, Moscow 117 813, Russia.

® Abstract published in *Advance ACS Abstracts,* October 1, 1994.

(1) (a) Ismail, A. A.; Sauriol, F.; Butler, I. S. *Inorg. Chem.* **1989**, *28*, 1007. Dombek, B. D.; Angelicio, R. J. *J. Am. Chem. Soc.* **1976**, *98*, 4110. Darensbourg, D. J. *Inorg. Chem.* **1979**, *18*, 14. Darensbourg, D. J.; Baldwin, B. J. *J. Am. Chem. Soc.* **1979**, *101*, 6447. Darensbourg, D. J.; Kudaroski, R.; Schenk, W. *Inorg. Chem.* **1982**, *21*, 2488. VanCatledge, F. A.; Ittel, S. D.; Jesson, J. P. *Organometallic* **1985**, *4*, 18. Bond, A. M.; Carr, S. W.; Colton, R. *Organometallics* **1984**, *3*, 541. (b) Darensbourg, D. J.; Gray, R. L. *Inorg. Chem.* **1984**, *23*, 2993.

(2) Muetterties, E. L. *J. Am. Chem. Soc.* **1968**, *90*, 5097. Bailar, J. C., Jr. *J. Inorg. Nucl. Chem.* **1958**, *8*, 165.

(3) Hoffmann, R.; Howell, J. M.; Rossi, A. R. *J. Am. Chem. Soc.* **1976**, *98*, 2484.

(4) (a) Jessop, P. G.; Morris, R. H. *Coord. Chem. Rev.* **1992**, *121*, 155. (b) Heinekey, D. M.; Oldham, W. J., Jr. *Chem. Rev.* **1993**, *93*, 913. (c) Günzburg, A. G.; Bagatur'yants, A. A. *Metallorg. Khim.* **1989**, *2*, 249.

(5) Bianchini, C.; Mealli, C.; Peruzzini, M.; Zanobini, F. *J. Am. Chem. Soc.* **1987**, *109*, 5548.

(6) Johnson, B. F. G.; Segal, J. A. *J. Chem. Soc., Dalton Trans.* **1974**, 981.

(7) Packett, D. L.; Trogler, W. C. *J. Am. Chem. Soc.* **1986**, *108*, 5036.

0276-7333/94/2313-4203$04.50/0 

**Table 1. Kinetic Parameters of the H/H Ligand Exchanges in Complexes 1–4[a]**

| compd no. | solvent | $\tau = 1/k$ (S) | $T$ (°C) | $E_a$ (kcal/mol) | $\Delta H^{\ddagger}$ (kcal/mol) | $\Delta S^{\ddagger}$ (eu) | $\Delta G^{\ddagger}(333)$ (kcal/mol) |
|---|---|---|---|---|---|---|---|
| **1** | toluene-$d_8$ | 1.2 | 60 | 19.1 ± 0.2 | 18.4 ± 0.2 | −3.7 ± 1.0 | 19.6 ± 0.2 |
| **1** | toluene-$d_8$/DMSO-$d_6$ (1:1) | 2.4 | 60 | 19.4 ± 0.5 | 18.7 ± 0.5 | −3.9 ± 1.2 | 20.0 ± 0.25 |
| **2** | toluene-$d_8$ | 0.95 | 60 | 21.1 ± 0.7 | 20.5 ± 0.7 | 2.3 ± 1.8 | 19.7 ± 0.2 |
| **3** | toluene-$d_8$ | 0.57 | 60 | 15.9 ± 0.4 | 15.2 ± 0.4 | −12.4 ± 2.2 | 19.3 ± 0.2 |
| **4** | toluene-$d_8$ | 0.055 | 60 | 15.2 ± 0.2 | 14.6 ± 0.2 | −9.1 ± 0.6 | 17.6 ± 0.2 |
| | | 0.15 | 45 | | | | |
| **4** | toluene-$d_8$/DMSO-$d_6$ (1:1) | 0.2 | 45 | 14.2 ± 1.0 | 13.6 ± 1.0 | −13.3 ± 3.0 | 17.8 ± 0.3 |

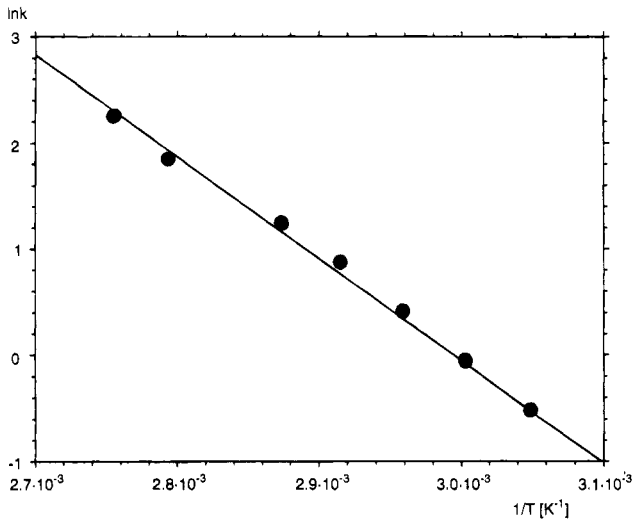


**Figure 1.** ln $k$ vs $1/T$ plot for the H/H exchange process of **1** in toluene-$d_8$.

revealed a pseudooctahedral coordination geometry. Even though the two hydride atoms could not be located, it was clear from the position of the "holes" in the coordination sphere that they are cis to each other. The heavy atoms around the Re center show significant dislocations from an ideal octahedral arrangement; i.e. the phosphorus donors of **4** "lean over" toward the hydrogen atoms (P—Re—P angle ~160 °), and the angle of the "equatorial" ligands is somewhat widened up to 102.5°. The $\pi$-acceptor versus $\sigma$-donor site preference of ligands in the pseudooctahedron of **4** (CO and NO trans to H, phosphorus donors cis to H) and the distortion toward a bicapped-tetrahedral geometry are in accord with the predictions from a quantum-mechanical analysis.[3]

For complexes **1**, **3**, and **4** the $r_{H_a\cdots H_b}$ and $r_{Re-H_{a,b}}$ distances as well as the $H_a$—Re—$H_b$ angles have been obtained from $T_{1,min}$ $^1$H relaxation time measurements in solution using the approach of separating selective, biselective, and nonselective relaxation time contributions.[11] ($r_{H_a\cdots H_b}$/$H_a$—Re—$H_b$ (Å/deg): 2.34/86 (**1**), 2.25/81 (**3**), 2.28/83 (**4**)). The OC—Re—$H_a$,$H_b$ angles can be assumed to be close to 180 and 90°, respectively, since for **1** an approximate 1:2 ratio of the $J(O^{13}C,H_b)$/$J(O^{13}C,H_a)$ coupling constants (5.5/12 Hz) was found in selectively decoupled $^{13}$C NMR spectra.

Summarizing these structural data, it is reasonable to describe the ground states of **1**–**4** as classical dihydride complexes with deviations from the octahedral coordination geometry toward a bicapped tetrahedron.

**Variable-Temperature NMR Experiments.** Variable-temperature $^1$H NMR spectra and $^1$H NMR saturation transfer data of **1**–**4** revealed stereochemical nonrigidity in solution manifested by H/H ligand exchange between 40 and 90 °C. From standard $^1$H NMR saturation transfer experiments and ReH $T_1$ relaxation time measurements[12] temperature-dependent rate constants (plotted in a representative way for **1** in Figure 1) and activation parameters of the exchange process (Table 1) have been obtained.

There is satisfactory evidence for an intramolecular exchange and, hence, a nondissociative mechanism supported by the following observations.

(A) The $^1$H NOESY experiment[8b] for the metal-bound protons in **2** given in Figure 2 showed line correlation in toluene-$d_8$ at 65 °C as presented schematically:

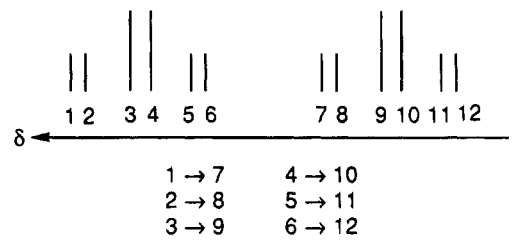


This allows us to establish an intramolecular exchange of the H ligands.

(B) The $ReH_aH_b$ $^1$H NMR resonances of **4** are broadened in toluene-$d_8$ at 50 °C due to the H ligand exchange, which is comparable to the NMR time scale (300 MHz). No changes in line widths and therefore in rate constants were observed when excess $P(OiPr)_3$ was added. This suggests that exchange between coordinated and noncoordinated phosphorus donors does not occur.

(C) Incorporation of $^{13}$CO, indicative of a $^{13}C/^{12}C$ exchange, was not observed in $^{13}$C NMR spectra of a toluene solution of **3** under 1 atm of $^{13}$CO.

(D) For a solution of **4** in toluene-$d_8$ no incorporation of $D_2$ (1.5 atm) was observed at ambient temperature or at 40 °C, ruling out a reductive-elimination/oxidative-addition route as an intermolecular exchange alternative (cf. (A)).

(E) The kinetic data for **1**–**4** reveal slightly negative or nearly zero values for the entropy of activation, which do not support the idea of a dissociative intimate mechanism. For an associative exchange reaction as the other intermolecular mechanistic alternative the $\Delta S^{\ddagger}$ values are too low in their negative magnitude.

(F) Bimolecular associative pathways can also be ruled out from concentration-dependent $^1$H NMR in-

(8) (a) Meakin, P.; Guggenberger, L. J.; Jesson, J. P.; Gerlach, D. H.; Tebbe, F. N.; Peet, W. G.; Muetterties, E. L. *J. Am. Chem. Soc.* **1970**, *92*, 3482. Gerlach, D. H.; Peet, W. G.; Muetterties, E. L. *J. Am. Chem. Soc.* **1972**, *94*, 4545. Meakin, P.; Muetterties, E. L.; Tebbe, F. N.; Jesson, J. P. *J. Am. Chem. Soc.* **1971**, *93*, 4701. Meakin, P.; Muetterties, E. L.; Jesson, J. P. *J. Am. Chem. Soc.* **1973**, *95*, 75. (b) Ball, G. E.; Mann, B. E. *J. Chem. Soc., Chem. Commun.* **1992**, 561.

(9) Field, L. D.; Bampos, N.; Messerle, B. A. *Magn. Reson. Chem.* **1991**, *29*, 36.

(10) Hund, H.-U.; Ruppli, U.; Berke, H. *Helv. Chim. Acta* **1993**, *76*, 963.

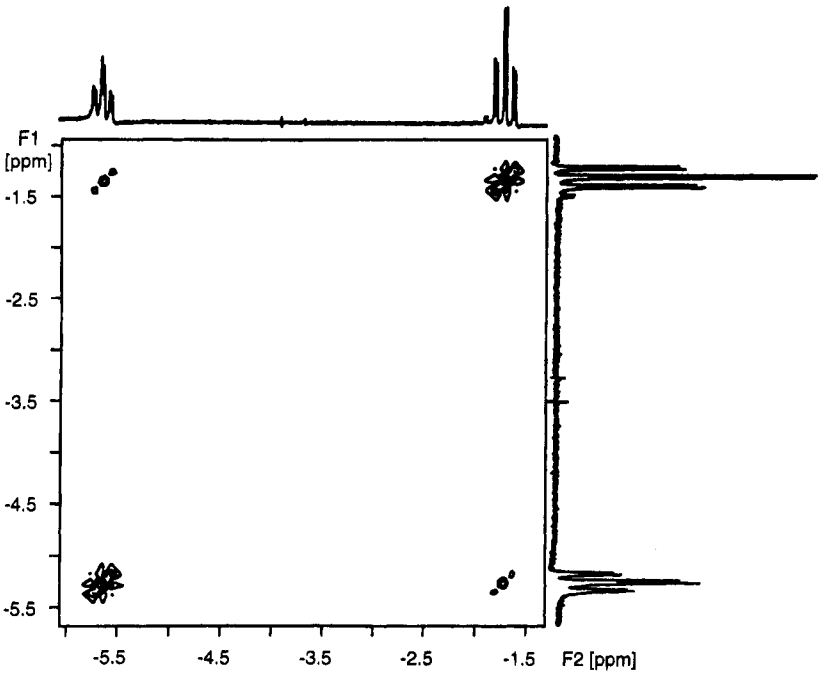


**Figure 2.** $^1$H NOESY experiment for **2** in toluene-$d_8$ at 65 °C.

**Scheme 1**[a]

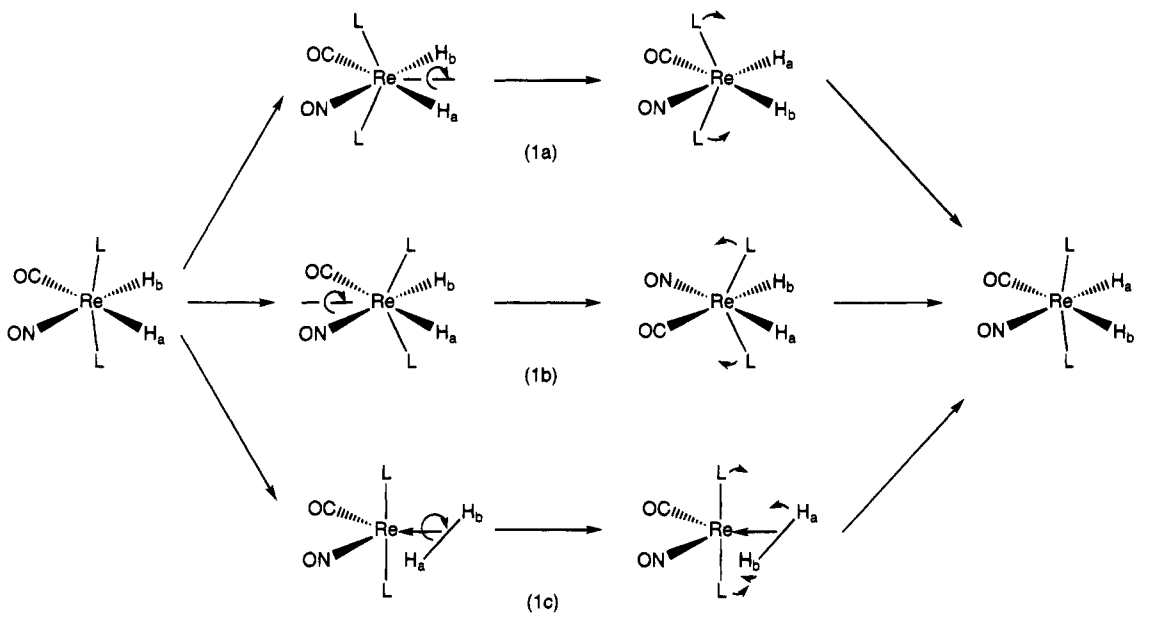


[a] L = phosphorus donor.

vestigations of **1**. Raising the concentration at 55 or 60 °C up to a 4-fold value compared to those for the kinetic measurements of Table 1 did not change the corresponding reaction rates.

In none of the NMR experiments on **1**–**4** have any new pseudooctahedral isomers been observed (within the NMR detection limits). Therefore, a degenerate kinetic behavior is required for the H/H exchange reactions, since the starting compounds and the products are the same. This condition cannot be satisfied by either of the bicapped-tetrahedral pathways with 90° rotation of a tetrahedral axis or by the trigonal-twist and the tetrahedral-jump processes. The H ligand scrambling could, however, pass through bicapped-tetrahedral intermediates with subsequent 180° rotation of appropriate tetrahedral edges made up by the CO and NO or by the $H_a$ and $H_b$ ligands (Scheme 1; eqs 1a and 1b). Alternatively, a dihydride/dihydrogen rearrangement with formation of a trigonal-bipyramidal nonclassical $H_2$ complex could take place, allowing almost free rotation of the $H_2$ moiety, which is a typical feature of the $\eta^2$-$H_2$ ligand[13] (eq 1c).

For the process in eq 1a the phosphorus donors are required to be pulled strongly backward from the $H_2$ ligand to achieve a bicapped tetrahedron, in which the $\pi$-acceptor ligands CO and NO represent the caps of the

(11) Gusev, D. G.; Nietlispach, D.; Vymenits, A. B.; Bakhmutov, V. I.; Berke, H. *Inorg. Chem.* **1993**, *32*, 3270.

(12) (a) Forsen, S.; Hoffmann, R. A. *J. Chem. Phys.* **1963**, *32*, 2892. (b) Freeman, R. A. *Handbook of Nuclear Magnetic Resonance*; Wiley: New York, 1988; pp 198–202. (c) Kaplan, J. H.; Fraenkel, G. *NMR of Chemically Exchanging Systems*; Academic Press: New York, 1980; p 153.

**Table 2. Dependence of ln $k$ for the H/H Exchange Processes of 1–4 (60 °C) on the Electronic and Steric Factors of the $PR_3$ Groups and $\nu$(CO) and $\nu$(NO)**

| compd no. | ln $k$ | $\chi$ ($cm^{-1}$) | cone angle (deg) | $\nu$(CO) ($cm^{-1}$) | $\nu$(NO) ($cm^{-1}$) |
|---|---|---|---|---|---|
| **1** | −0.182 | 1.40 | 170 | 1945 | 1623 |
| **2** | 0.0513 | 3.45 | 160 | 1957 | 1650 |
| **3** | 0.562 | 8.55 | 118 | 1966 | 1655 |
| **4** | 2.90 | 19.05 | 130 | 1997 | 1671 |

tetrahedron and the rotating edge is given by the two metal-bound H atoms. For a mechanism according to eq 1b it is necessary to dislocate the phosphorus groups towards $H_a$ and $H_b$ as the tetrahedral caps, extending the natural distortion coordinate of **1–4**. Subsequently there is rotation of the CO/NO edge. The rearrangement in eq 1c is distinguished from a bicapped-tetrahedral pathway, in that the phosphorus donors are placed in approximately axial positions and the hydrogen atoms are brought together to form the dihydrogen moiety.

Other indirect evidence can be used to distinguish between the intramolecular exchanges and as an indication that the reaction might proceed via the mechanism sketched in eq 1c. There is a considerable dependence of the rate constants and the exchange barriers on the electronic factors of the $PR_3$ groups. The data for **1–4** listed in Table 2 show a positive linear correlation of ln $k$ vs the electronic parameters $\chi$[14] and ln $k$ vs $\nu$(CO) values (Figure 3). The correlation between ln $k$ vs $\nu$(NO) is not as straight, presumably due to a varying amount of coupling between $\nu$(MH) and $\nu$(NO). We have observed coupling of this type in tungsten complexes.[15]

The data of Table 2 and Figure 3 indicate that the transition states of these processes are stabilized more, if less donating and better $\pi$ accepting phosphorus ligands are present. In addition, the CO groups as well as the NO ligands in their "equatorial" positions of **1–4** are expected to assist a process of charge withdrawal which is required for the stabilization of transition states or intermediates of in the mechanism of eq 1c, since the formal oxidation state of the rhenium center is lowered from +1 in **1–4** to −1 in such species. Effective charge delocalization also would help to keep the difference in charge distribution between ground and transition states small. As a consequence, one would expect a reduced solvent dependence of the rate constants. In fact, it was found that the activation parameters of the exchanges are practically the same in nonpolar toluene and in a polar mixture of toluene and DMSO (1:1) (Table 1).

In a further interpretation of the data in Table 2, it is noteworthy that there is apparently no obvious correlation between rate constants and steric factors of the $PR_3$ moieties, which strongly indicates that the rearrangements of **1–4** are dominated by electronic influences.

Dihydride/dihydrogen exchange processes would be expected to resemble reductive eliminations of $H_2$[16] in their intimate mechanisms, since the latter reactions presumably proceed via the formation of $H_2$ complexes as the rate-determining step. Hence, it seems appropriate to compare $k_H/k_D$ values of reductive $H_2/D_2$ eliminations with the deuterium isotope effects for the H/H exchange processes in **1** and **4**. These showed practically no kinetic isotope effect ($k_H/k_D$ = 1.07 and 1.13, respectively) in $^1$H NMR saturation transfer spectra of mixtures of $ReH_2$ and ReHD isotopomers in toluene-$d_8$. For reductive $H_2/D_2$ eliminations three categories of isotope effects[17a] have been observed: it is possible to have a normal, no, and an inverse isotope effects, which correspond to early, middle, and late transition states of these transformations. In accord with our MO calculation presented later (the H···H contact according to the calculations is 1.24 Å; see Table 3), a middle transition state along the pathway of eq 1c is proposed. This becomes even more plausible, since our calculations indicate that the $H_2$ complex intermediate is in an energetic vicinity range of the ground state. In the related system $W(CO)_3H_2(PCy_3)_2$, interconversions of the observable dihydride and dihydrogen species differ in reaction enthalpy by only 0.8 kcal/mol. They are separated, however, by a relatively high kinetic barrier of 16 kcal/mol.[17b] The reaction coordinate of the latter process resembles the proposed H/H exchange mechanism of **1–4**, and it is therefore not surprising that for the tungsten dihydride/dihydrogen conversion a small deuterium isotope effect of only 1.08[17b] is observed also. Since for an H/H exchange mechanism according to eq 1a, with migration of the H ligands through the P—Re—P plane, a significant normal deuterium isotope effect may be expected, it is deemed unlikely that this reaction path is operative for the rearrangements of **1–4**. However, by the mechanism of eq 1b a small $k_H/k_D$ effect should also result, since the crucial bond changes do not involve the Re—H bonds. If just the kinetic isotope criterion were applied, this mechanism would be indistinguishable from the discussed specific situation of eq 1c.

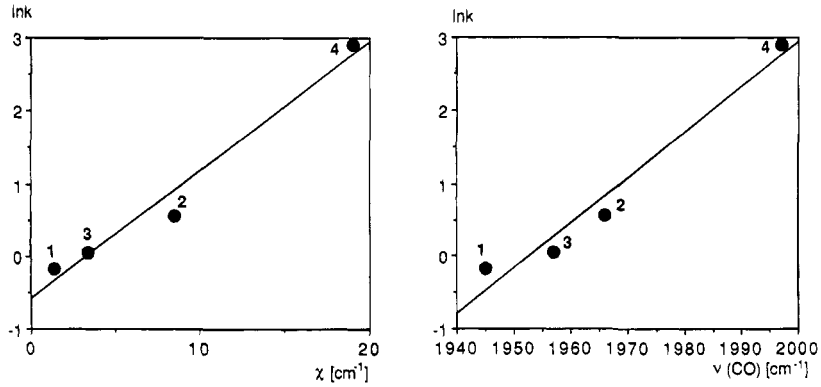


**Figure 3.** Plots of ln $k$ vs Tolman's parameters (left) and of ln $k$ vs $\nu$(CO) ($cm^{-1}$) (right) for **1–4**.

**Table 3. Structural Parameters of the Species 4–7, 5T–7T, 5I–7I, and 5TR–7TR**

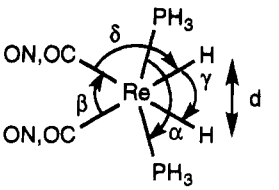


| | 4 | 5 | 6 | 7 | 5T | 6T | 7T | 5I | 6I | 7I | 5TR | 6TR | 7TR |
|---|---|---|---|---|---|---|---|---|---|---|---|---|---|
| α (deg) | 159.4 | 169 | 167 | 172 | 178 | 174 | 178 | 178 | 177 | 180 | 179 | 178 | 117 |
| β (deg) | 102.5 | 95 | 95 | 94 | 126 | 123 | 131 | 140 | 136 | 144 | 140 | 136 | 178 |
| γ (deg) | 83 | 84 | 83 | 86 | 42 | 44 | 41 | 24 | 24 | 25 | 24 | 24 | 25 |
| δ (deg)[a] | | 94 | 91 | 90 | 112 | 96 | 94 | 120 | 100 | 95 | 131 | 102 | 89 |
| ϵ (deg)[b] | 0 | 0 | 0 | 0 | 0 | 0 | 0 | 0 | 0 | 0 | 90 | 90 | 90 |
| *d*(H–H) (Å) | 2.28 | 2.28 | 2.25 | 2.32 | 1.24 | 1.30 | 1.21 | 0.72 | 0.72 | 0.74 | 0.72 | 0.72 | 0.74 |

[a] ON–Re–H angle. [b] ϵ = (Re(CO,NO)(CO,NO))–(ReH$_2$) angle.

The interpretation of the close to zero (**1**, **2**) or moderately negative $\Delta S^{\ddagger}$ values (**3**, **4**) (Table 1) toward any mechanistic alternative is certainly difficult, especially in view of the fact that there is only one related literature report for the $\Delta S^{\ddagger}$ value of a dihydride/dihydrogen transformation.[18] The W(CO)$_3$(PiPr$_3$)$_2$H$_2$ complex rearranges to the corresponding nonclassical (H$_2$) species with a $\Delta S^{\ddagger}$ value of −21 eu, which is somewhat more negative than those of the H/H exchange processes of the comparably phosphine substituted compounds **1** and **3**. For the rearrangement reaction of FeH$_2$[P(OEt)$_3$]$_4$ a $\Delta S^{\ddagger}$ value of −8.8 eu was determined.[8a] This process was found, however, to follow the tetrahedral jump mechanism. With one exception,[1b] for which $\Delta S^{\ddagger} = -54.9$ eu was measured, nondissociative isomerizations of non-hydride-containing complexes[1a] show $\Delta S^{\ddagger}$ values between +10 and −28 eu.

While there are to our knowledge no literature reports which suggest the dynamic behavior of hydride complexes to proceed along the lines of eqs 1a and 1b, H/H exchange with the transformation of a d$^6$ octahedron to a d$^8$ trigonal bipyramid according to eq 1c has been shown to occur in a [RhH$_2$(tetraphos)]$^+$ compound.[5] In addition there are a few d$^6$ ↔ d$^8$ Ir examples[19] of reductive H$_2$ eliminations in which dihydride/dihydrogen interconversions have been proposed as the initiating steps. This may, therefore, also give support to the idea that the rearrangements of **1**–**4** are operating on the basis of eq 1c.

As mentioned earlier, Ru(CO)H$_2$(PPh$_3$)$_3$ rearranges via the trigonal-twist and FeH$_2$[P(OEt)$_3$]$_4$ via a tetrahedral-jump mechanism. Obviously there is a subtle balance of electronic and steric factors which determines the energetic accessibility of suitable intermediates and transition states. The appearance of d$^8$ trigonal-bipyramidal H$_2$ complexes as intermediates or transition states in the fluxional processes of **1**–**4** seems to be linked to the presence of NO ligands.[4,20] Equation 1c is also given support as the reaction pathway for the H/H exchange of **1**–**4** by MO calculations, which are discussed in the following section.

**EHT Calculations.** Extended Hückel calculations were carried out to model the H$_a$/H$_b$ exchange processes of **1**–**4** shown in eqs 1a–c. Moreover, the ligand influence of the π-acceptor groups was probed.

With the dihydride complexes **5**–**7** as starting compounds, differing in the π-acceptor substitution patterns, computations were performed in a search for reaction paths of the mentioned transformations using MEHT model calculations.[21] While **5** is related to **1**–**4**, **6** and **7**

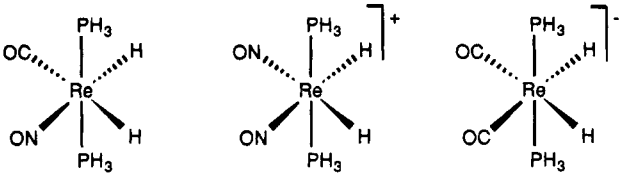


**5** **6** **7**

are artificial molecules. The latter have been introduced into the theoretical investigations for clear symmetry distinctions in the orbital analyses and for an unambiguous separation of the π-acceptor ligand influence. The Re–C, –N, and –P bond distances for the ground-state molecules **5**–**7** were adopted from the X-ray structure determination of **4**. Fixed Re–H, N–O, C–O, and P–H bond lengths have been used for all calculations, since in exploratory optimizations of **5**, experimental Re–X bond lengths were not well reproduced in our calculations (deviations: Re–C (−5%), Re–N (−6%), Re–P (+15%)).

Therefore, only angular optimizations were carried out on structures **5**–**7**, which led to the values given in Table 3. The basic structural features of **5**–**7** turned out to be grossly invariant to the nature of the π-acceptor ligands. In comparison to the angular parameters

(13) Eckert, J.; Kubas, G. J.; Dianoux, A. J. *J. Chem. Phys.* **1988**, *88*, 466. Eckert, J.; Jensen, C. M.; Jones, G.; Clot, E.; Eisenstein, O. *J. Am. Chem. Soc.* **1993**, *115*, 11056.
(14) Lin, H.-Y.; Eriks, K.; Prock, A.; Giering, W. P. *Organometallics* **1990**, *9*, 1758.
(15) Van der Zeijden, A. A. H.; Sontag, C.; Bosch, H. W.; Shklover, V.; Berke, H.; Nanz, D.; von Philipsborn, W. *Helv. Chim. Acta* **1991**, *74*, 1194.
(16) Hay, P. J. In *Transition Metal Hydrides*; Dedieu, A., Ed.; VCH: New York, 1992; pp 127–148.
(17) (a) Bullock, R. M. In *Transition Metal Hydrides*; Dedieu, A., Ed.; VCH: New York, 1992; pp 263–307. (b) Zhang, K.; Gonzalez, A. A.; Hoff, C. D. *J. Am. Chem. Soc.* **1989**, *111*, 3627. Gonzalez, A. A.; Zhang, K.; Nolan, S. P.; de la Vega, R. L.; Mukerjee, S. L.; Hoff, C. D. *Organometallics* **1988**, *7*, 2429.
(18) Gonzalez, A. A.; Zhang, K.; Mukerjee, S. L.; Hoff, C. D.; Khalsa, C. R. K.; Kubas, G. J. In *Bonding Energetics in Organometallic Compounds*; Marks, T. J., Ed.; American Chemical Society: Washington DC, 1990; pp 133–147.
(19) Burk, M. J.; McGrath, M. P.; Wheeler, R.; Crabtree, R. H. *J. Am. Chem. Soc.* **1988**, *110*, 5034.
(20) Burdett, J. K.; Eisenstein, O.; Jackson, S. A. *Transition Metal Hydrides*; Dedieu, A., Ed.; VCH: New York, 1992; pp 149–184.
(21) Anderson, A. B. *J. Chem. Phys.* **1975**, *62*, 1187. Pensak, D. A.; McKinney, R. J. *Inorg. Chem.* **1979**, *18*, 3407.

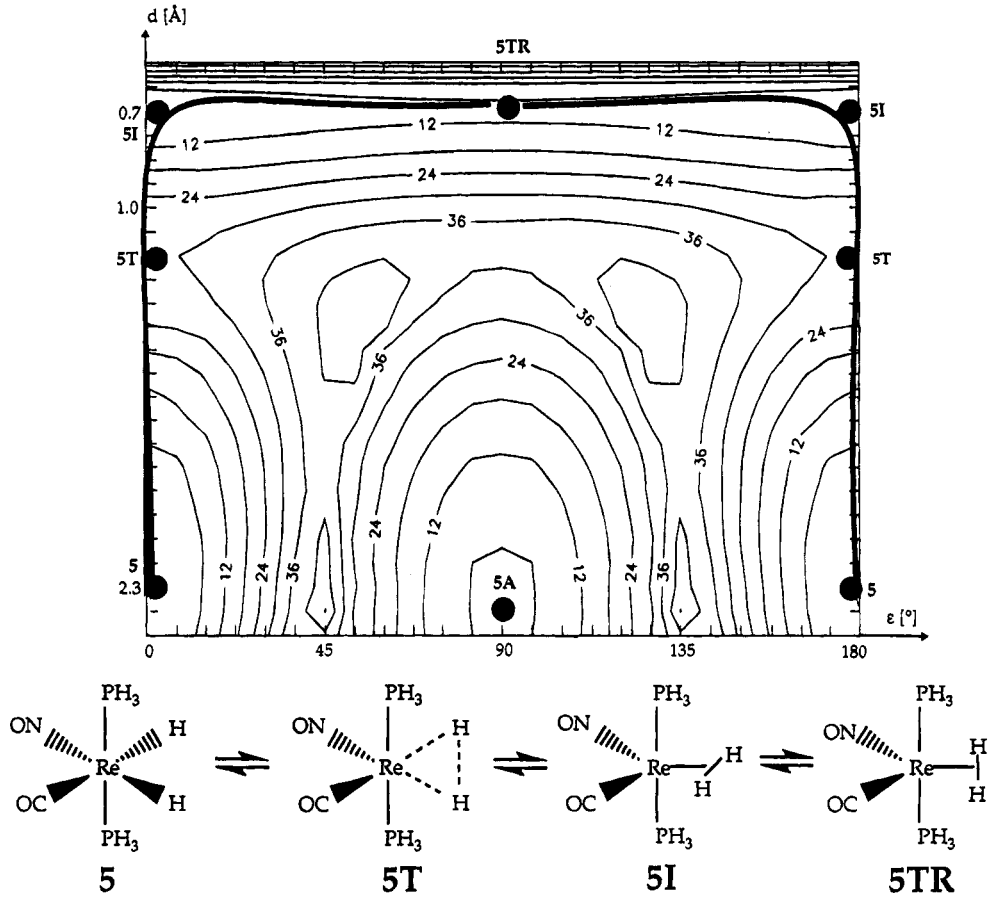


**Figure 4.** Contour plots for the multidimensional energy hypersurface (kcal/mol) and representation of the reaction path for the **5** → **5T** → **5I** → **5TR** conversion. The optimized degrees of freedom are described in Table 3. The energy zero is given by the ground-state molecule [Re(CO)$H_2$(NO)($PH_3$)$_2$] (**5**). The axes are denoted by the H—H distance $r$ and by the interplanar angle $\epsilon$ ((Re$H_2$)—(Re(CO)(NO))).

of **4**, only the α values of **5**–**7** showed significant deviations. This is presumably due to steric effects of the phosphorus ligands in **4**, which are not accounted for by the choice of $PH_3$ groups as model donors in the calculations.

Intramolecular rearrangements of pseudooctahedral compounds such as **1**–**4** could principally involve positional isomers as crucial intermediates. We have therefore optimized all five other isomers of **5**, which are local minima on the energy hypersurface. For this procedure the same degrees of freedom as for the optimization of **5**–**7** were used. The total energy differences of these isomers are 1.5–5 kcal/mol with respect to **5**, which suggests that the corresponding isomers of **1**–**4** could be energetically accessible and those with an energetic difference smaller than 3 kcal/mol could even be traceable in NMR experiments. It is noteworthy that the NMR spectra of **1**–**4** did not indicate the presence of any isomeric complexes. Consequently, principal kinetic barriers preventing their facile interconversion have to be assumed.

With the optimized geometries of **5**–**7** as starting points, cuts through the multidimensional rearrangement energy hypersurface were established for the interchange of the nonequivalent hydrogen atoms in **5** and the equivalent rhenium-bound hydrogen atoms in **6** and **7**. In each point of the energy surfaces α and β (and δ in the case of **5**) were optimized. The degrees of freedom used for the representations of the surfaces were the $d$(H—H) distance (implicitly $\gamma$) and $\epsilon$, the angle between the Re$H_2$ and the Re(CO,NO)(CO,NO) planes as defined in Table 3. Since all were found qualitatively to be very similar, only the hypersurface of the H/H exchange process of **5** is presented in Figure 4.

The energy hypersurfaces for all conversions show a mountainous area with relatively steep descents into two crossing, almost perpendicular, valleys. In addition, there are four saddle points and two local minima. Saddle points lying at lowest energy represent the transition states **5T**–**7T** (for structural parameters, see Table 3), separating the starting components **5**, **6**, and **7** from trigonal-bipyramidal intermediates **5I**–**7I**, with nonclassical $H_2$ structures being prominent resting states on these surfaces. Other saddle points localized in the horizontal valley stand for transition states of the $H_2$ rotation about the Re—($H_2$) axis (**5TR**–**7TR**).

The other local minima of these energy surfaces are the dihydride complexes **5A**–**7A**, bearing the phosphorus donors trans to the hydrogen ligands with the π-acceptor substituents in "axial" positions. The conversion of **5**–**7** to these compounds can occur on a bicapped-tetrahedral reaction coordinate (H/H axis rotating 90°) via saddle points lying 41, 37, and 48 kcal/mol above **5**–**7**. Since the value of the computed barrier for the transformation of **5** to **5A** is quite high and higher than that of the **5** to **5T** conversion, one might conclude that in the case of **1**–**4** the formation of geometric isomers is energetically not feasible. The energy hypersurfaces of the H/H exchanges of complexes **6** and **7** also show local minima for the trans NO/CO,

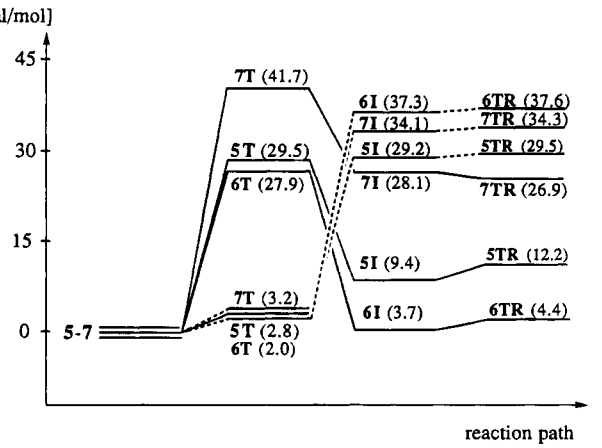


**Figure 5.** Schematic total (solid lines) and MEHT electrostatic energy (dashed lines) plots of the computed H/H exchange reaction paths of **5**–**7**.

cis $PH_3$ isomers **6A** and **7A**, which are also isolated by high kinetic barriers being the highest transitions of these surfaces. The computed energy hypersurface for

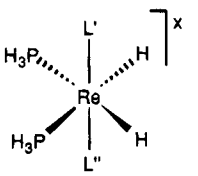


L' = CO, L" = NO, x = 0 **5A**
L' = L" = NO, x = 1+ **6A**
L' = L" = CO, x = 1- **7A**

the H/H exchange process of **5** reveals a reaction pathway analogous to that of eq 1c. The reaction proceeds from **5** to **5T** with a steep energetic increase and then descends to the intermediate **5I** with subsequent $H_2$ rotation passing through **5TR**. Similar conditions are computed for the H/H exchange reaction paths starting from **6** and **7**. A crossing to the dihydrogen complexes **6I** and **7I** via the transition states **6T** and **7T** allows $H_2$ rotation via **6TR** and **7TR**, which completes these rearrangements.

The reaction pathways for all H/H exchange processes of **5**–**7** are sketched in Figure 5 using the structures **5**–**7**, **5T**–**7T**, **5I**–**7I**, and **5TR**–**7TR** as prominent energetic points. From Figure 5 we can derive the following points.

(A) In comparison to the range of the experimental $\Delta H^{\ddagger}$ values of **1**–**4** (Table 1) the calculated barrier of the H/H exchange process of **5**, given by the energetic difference between **5** and **5T**, is too high. In view of the fact that the applied method did not allow proper optimizations of Re–X distances and that the optimized angular degrees of freedom have been restricted, the computed value of 27.9 kcal/mol is, however, still in an acceptable energetic range with regard to the experimentally determined energies. For the same reason the computed barriers for the H/H exchange processes of the unknown model complexes **6** and **7** are probably also somewhat too high. Figure 5 also shows the development of the MEHT electrostatic energies along the reaction paths. It can be seen that these contributions affect the ground- and transition-state structures to very similar extents. The nonclassical $H_2$ complexes (**5T-7T** and **5TR-6TR**) are, however, strongly destabilized mainly due to the H/H repulsion.

(B) The calculations show for all processes the existence of intermediates (**5I**–**7I**) representing nonclassical $H_2$ complexes in energetic vicinity to the ground-state structures **5**–**7**. Particularly the dinitrosyl derivative **6I** is a surprisingly stable species. It is only 3.7 kcal/mol above the ground state **6**.

(C) The computed barriers for the H/H exchange processes are markedly lower, if at least one NO ligand is present.

(D) With complexes **5I** and **6I** as starting points, the rotations of the $H_2$ ligands via **5TR** and **6TR** are minor energetic factors.[14] In the case of **7I** a combined pseudorotation of the ancillary ligands and rotation of the $H_2$ moiety leads to **7TR** (CO moieties axial, $PH_3$ groups equatorial, and $H_2$ parallel to the P–Re–P axis), which is even lower in energy than **7I** by 1.2 kcal/mol. (For a better comparison the labeling scheme used for **5** and **6** has been applied to **7** also.)

The calculated structural features of the species **5T**–**7T**, **5I**–**7I**, and **5TR**–**7TR** are given in Table 3. In a first approximation the structures of all these species may be described as trigonal bipyramids. The axial ligands have an angle of about 180°. In **5I**–**7I** and **5TR** and **6TR** the equatorial angles between the $\pi$-acceptor ligands are slightly widened with respect to an ideal tbp geometry. This effect will be traced by the orbital analysis in the later context. The H–H distances of **5T**–**7T** represent weak contacts, while those of **5I**–**7I** and **5TR**–**7TR** are typical of $H_2$ ligands in transition-metal complexes.[4]

The computations in the search for reaction paths of the H/H exchange processes of **5**–**7** have so far been restricted to reaction pathways according to eq 1c and one type of bicapped-tetrahedral rearrangement involving the H/H axis as the rotating tetrahedral axis (eq 1a). We have completed the search for more favorable energetic pathways by probing all possible bicapped-tetrahedral trigonal-twist and tetrahedral-jump transformations of **5**. This includes the process according to eq 1b and also topological rearrangements leading to the other conceivable isomers of **5**. For the computations of the bicapped-tetrahedral hypersurfaces the same degrees of freedom as that of Figure 4 were used, e.g. with fixed bond lengths but with allowance for relaxation of relevant bond angles. For the rotations of opposite octahedral faces along the trigonal twist mechanism, the corresponding Re–ligand vectors of one face were rotated simultaneously. Because of its low symmetry the tetrahedral-jump path requires the optimization of quite a few angular degrees of freedom as given in the Experimental Section. The "hopping" of a hydride ligand from one tetrahedral face to another can occur through a $PH_3$/NO or $PH_3$/CO axis.

The results of these calculations are given in Table 4. They demonstrate quite high energetic barriers, for the bicapped-tetrahedral, the trigonal-twist, and the tetrahedral-jump mechanisms. This suggests that these processes are not competitive with the dihydride/dihydrogen rearrangement route in the fluxional molecules **1**–**4**, preventing the formation of geometrical isomers of them.

Figure 6 represents schematic orbital correlation diagrams for the transformations of the more symmetric molecules **6** → **6I** and **7** → **7I**, which are given in order to evaluate the effect of the strong $\pi$ acceptor NO. It should be emphasized that the sum of one-electron energies of Figure 6 is not equivalent to the total

**Table 4. Representation of Hydride Isomerization Pathways of 5 and Their Computed Activation Energies[a]**

Bicapped tetrahedron

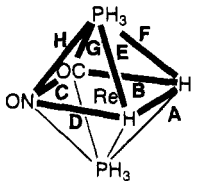


| Rotating tetrahedral axis | Computed activation energy [kcal/mol] |
|---|---|
| A | 41.3 |
| B | 39.2 |
| C | 46.1 |
| D | 43.8 |
| E | 36.9 |
| F | 41.5 |
| G | 39.2 |
| H | 39.2 |

Trigonal twist

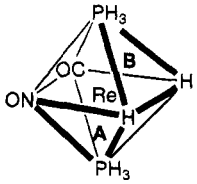


| Rotation face, 120/-120° | Computed activation energy [kcal/mol] |
|---|---|
| A, 120° | 46.1 |
| A, -120° | 44.3 |
| B, 120° | 46.1 |
| B, -120° | 48.9 |

Tetrahedral jump

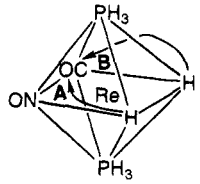


| migration path | Computed activation energy [kcal/mol] |
|---|---|
| A ($PH_3$/NO tetrahedral edge) | 47.2 |
| B ($PH_3$/CO tetrahedral edge) | 48.4 |

[a] The geometrical optimizations were carried out as given in the Results and Discussion or in the Experimental Section.

energies given in Figure 5, since the latter also contain MEHT electrostatic energy contributions, as mentioned before. The general trends of the energetic changes along the calculated MEHT reaction paths are, however, mirrored in the orbital pictures, which justifies their use in the interpretation of the ligand effect.

It can be immediately recognized that the orbital conversions of Figure 6 show qualitatively great resemblance with reductive eliminations of $H_2$ from $d^6$ pseudooctahedral dihydride complexes.[16] A general bookkeeping of the filled levels for the conversion of an octahedron ($d^6$) to a trigonal bipyramid ($d^8$) shows that the six $\sigma$ ($a_1$, $e_g$, $t_{1u}$) and three $\pi$ ($t_{2g}$) functions should transform into five $\sigma$ ($2a_1'$, $a_2''$, e'), two nonbonding $\pi$ (e''), and two slightly $\sigma$ antibonding $\pi$ type (e') orbitals, the last at somewhat elevated energy.[22]

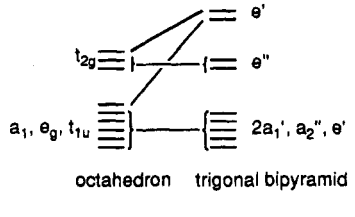


If symmetry allows such a transformation, and according to Figure 6 this is so for compounds **6** and **7** (and naturally for **5** also), one is left with the problem that one $\sigma$ and one $\pi$ orbital of the octahedron go into e' accompanied by an uncomfortable raise in energy. In the case of the dihydride/dihydrogen complex conversion one finds the special situation that the $\sigma$-orbital carrying character of the $H_2$ ligand appears in the trigonal-bipyramidal structure at relatively low energy and therefore can help to compensate part of the energetic destabilization of e'. The total energetic balance for a dihydride/dihydrogen complex transformation would, however, normally stay unfavorable; if not, other specific factors may have additional influence.

Getting back to the interpretation of the more detailed situation in Figure 6, the expected three orbital transformations with prominent rises or descents in energy forming e' or the lower lying $H_2$ orbitals are identified as the $9a_1$ (**6** and **7**), the $6b_2$ (**6**) or the $5b_2/6b_2$ (**7**), and the $8a_1/4a_1$ (**6**) or the $8a_1$, $7a_1/4a_1$ (**7**) transitions, respectively. In the case of compound **7**, the major part of the $\sigma_{M-H}$ character is localized in the $5b_2$ function and lies energetically below $\sigma_{CO}$, causing eventually an avoided crossing situation for the $5b_2/6b_2$ orbitals as the $\sigma_{M-H}$ character of $5b_2$ moves to a higher energy. Similarily, the H orbital character of $8a_1$ in **6** descends over several avoided crossings ($7a_1$, $6a_1$, $5a_1$) to $4a_1$. Related $a_1$ orbital changes are observed for the **7** → **7I** conversion, differing only in the participation of the $\sigma_{M-H}$ orbital character in $8a_1$ and prevailing in $7a_1$ of **7**.

Searching for energetically dominating orbital effects in the molecular conversions **6** → **6T** → **6I** and **7** → **7T** → **7I**, one finds that the total energy differences between these pathways can almost exclusively be related to the changes in $9a_1$ and $6b_2$ (**6**) or $6b_2/5b_2$ (**7**). Of both **6** and **7** the lower lying $a_1$ functions transform with about the same gain in energy. They are therefore not discussed in further detail. Focusing on the $6b_2$ and $6b_2/5b_2$ functions of both molecular transformations, an initial steep energetic increase with a flattening toward the end of these processes is noted. The shape of these curves is determined by four orbital contributions. The raise in energy results from the enhancement of the antibonding H/H interaction along the transformation path. This is, however, partly compensated by admixture of the energetically descending $8b_2$ $\sigma^*_{M-H}$ metal orbital character, which is released upon loss of $MH_2$ overlap. Additionally there is admixture of the $\pi^*$ orbitals ($7b_2$) of the acceptor ligands (CO, NO), which is promoted by an increasing angle between them along the reaction paths. For the NO system, however, the $7b_2$ level is energetically lower lying, which in turn leads to greater stabilization. For a visualization of the greater $\pi$-acceptor content in **6I**, plots of the filled $6b_2$ functions of **6I** and **7I** are shown in Figure 7. The different energetic behavior of the $6b_2$ and $5b_2/6b_2$ transformations can finally also be related to the lower energetic position of $5b_2$ in **7**.

This is explained best by partitioning of the $ReH_2(PH_3)_2(\pi\text{-acceptor})_2$ molecules into a $ReL_4$ and an $H_2$ fragment. $C_{2v}$ $ML_4$ units have two blocked sets of orbitals, with three of them at lower and two at higher energy.[22] Those two at higher energy ($a_1$ and $b_2$) are used for the binding of the two H atoms in **6** and **7**. Mainly due to the lower overlapping capability in **6**, which is caused by a stronger $\pi$-acceptor participation and hence diminished rhenium character (see Figure 8), there is weaker interaction of the $b_2$ fragmental lobe with the H atoms resulting in a $\sigma_{M-H}$ orbital at higher energy.

Again, the energetic behavior of $9a_1$ along the reaction paths is less favorable for the **7** → **7I** compared with

(22) Albright, T. A.; Burdett, J. K.; Whangbo, M.-H. *Orbital Interactions in Chemistry*; Wiley-Interscience: New York, 1985.

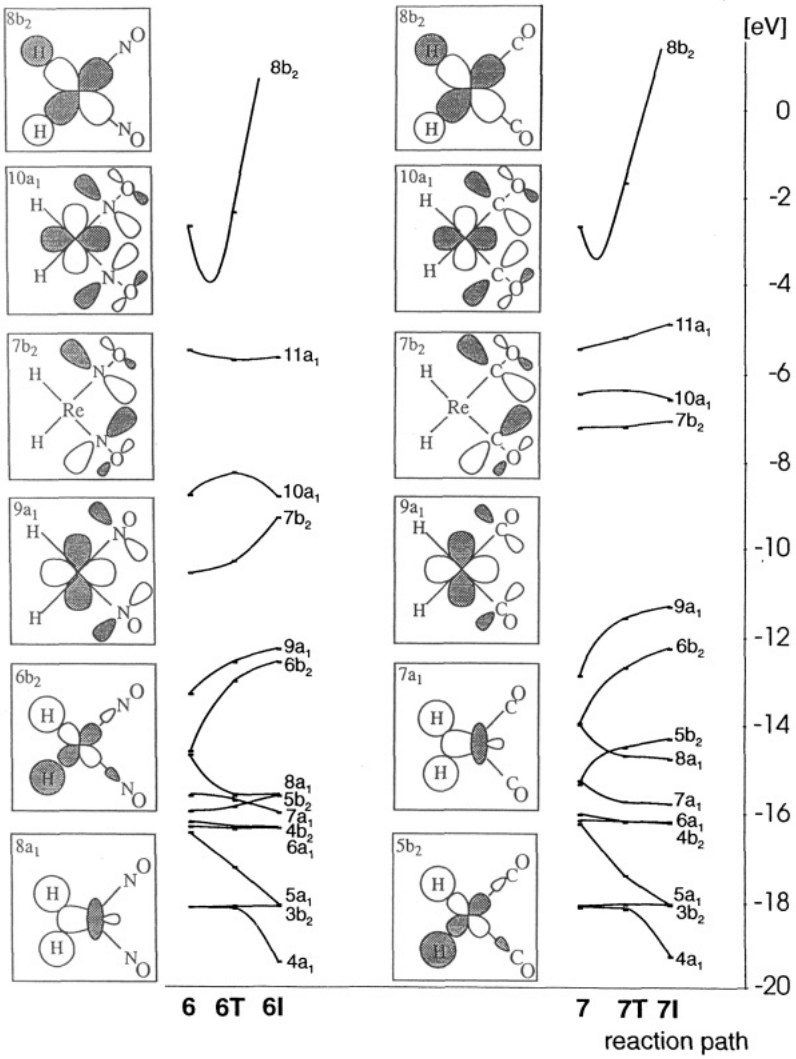


**Figure 6.** Orbital correlation diagrams for the $a_1$ and $b_2$ orbital conversions of the reaction paths **6** → **6T** → **6I** and **7** → **7T** → **7I**. The HOMOs are the $9a_1$ functions. The $a_2$ and $b_1$ transformations do not show significant energy changes along the reaction coordinate and are therefore omitted for clarity.

the **6** → **6I** process. This phenomenon can be rationalized by a similar fragmental orbital picture partitioning the $Re(H_2)(PH_3)_2(\pi\text{-acceptor})_2$ molecules of **6I** and **7I** into $ReL_4$ and $H_2$ fragments. Among the five orbitals of the rhenium unit there are two of the $a_1$ type.[22] Restricting ourselves to the $a_1$ part of a qualitative interaction scheme for **6I** and in **7I**, it can be seen that $9a_1$ has a nonbonding character.

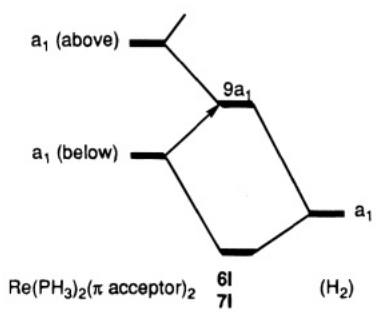


$9a_1$ bears a great deal of repulsive and therefore destabilizing interaction between the $a_1$(below) and $a_1$-$(H_2)$ FMOS. This is more pronounced in compound **7I**. The origin of the destabilization can be recognized from the shapes of the $a_1$(below) orbitals of the isoelectronic $[Re(NO)_2(PH_3)_2]^+$ and the $[Re(CO)_2(PH_3)_2]^-$ moieties of **6I** and **7I** shown in Figure 8.

In the nitrosyl-substituted compounds the lobe which is directed toward interaction with the $H_2$ units is more contracted and hence has less overlapping capability. The strong nitrosyl contribution leads to delocalization and therefore reduction of the Re character in this orbital. From a visual comparison of the $9a_1$ functions in **6I** and **7I**, presented in Figure 7, the greater Re—-$(H_2)$ repulsion in **7I** can easily be derived.

This orbital analysis of the $a_1$ and $b_2$ functions in the **6** → **6T** → **6I** and **7** → **7T** → **7I** transformations elucidates that the nitrosyl ligand participates energetically favorably in all crucial orbital conversions. The amount of stabilizing admixtures from the NO or CO $\pi^*$ levels depends on their energetic positions relative to those of the metal orbitals. Since the $\pi^*_{NO}$ orbitals in **6** are lower lying than the $\pi^*_{CO}$ orbitals in **7** and are also closer to the rhenium d levels, greater energetic stabilization results for the molecular conversion of the nitrosyl complex.

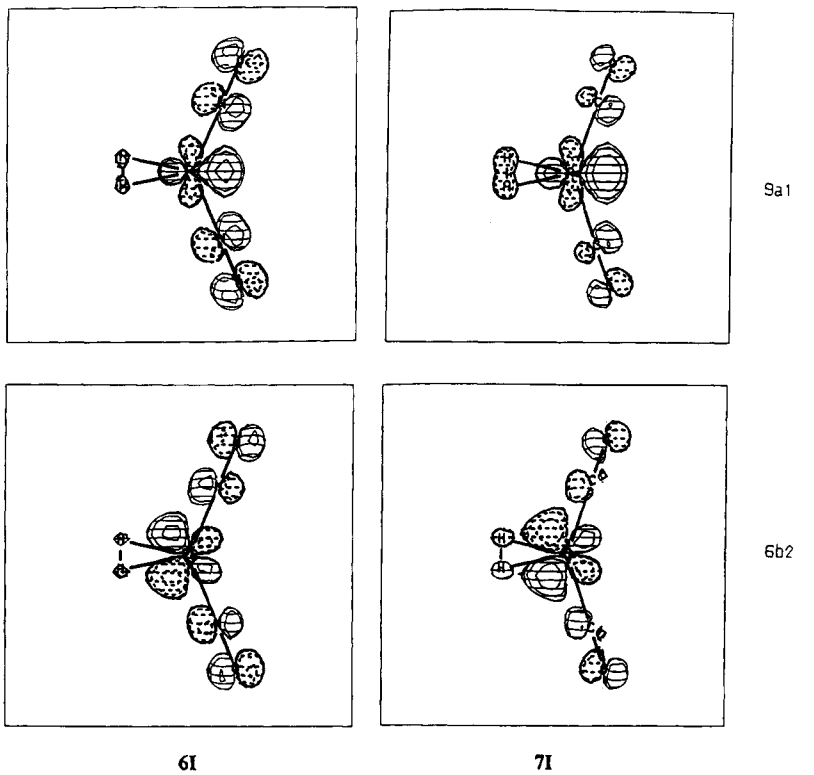


**Figure 7.** CACAO orbital plots[23] of the $7b_2$ and $9a_1$ functions in **6I** and **7I**, shown in the Re($\pi$-acceptor)$_2$ planes.

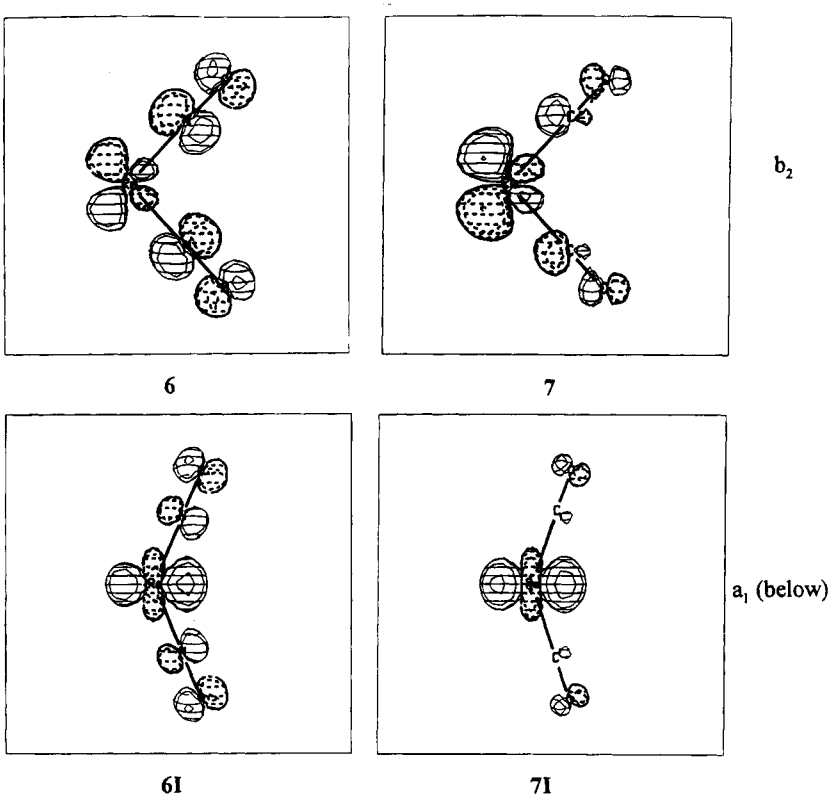


**Figure 8.** CACAO orbital plots[23] of the $b_2$ (**6** and **7**) and $a_1$(below) (**6I** and **7I**) functions of the $C_{2v}$[Re(NO)$_2$(PH$_3$)$_2$]$^+$ and the [Re(CO)$_2$(PH$_3$)$_2$]$^-$ fragments viewed in the Re($\pi$-acceptor)$_2$ planes.

## Experimental Section and Details of the Calculations

All manipulations were performed under a dry nitrogen atmosphere by standard techniques. Solvents were dried and deoxygenated by conventional procedures and were freshly distilled before use.

$^1$H and $^{13}$C NMR spectra were obtained on a Varian Gemini-300 spectrometer (300 MHz, $^1$H). $^1$H NMR saturation transfer experiments were performed by using standard techniques of the spectrometer.[12] The rate constants of the H/H exchanges ($k$) were calculated from the equation $A(S)/A(0) = 1/(1 + kT_1)$, where $A(S)$ and $A(0)$ correspond to the relative integral intensities of the H ligand signal with and without saturation

of the field.[12a,b] $T_1$ is the spin/lattice relaxation time of this nucleus. The intensities $A(0)$ were taken from three to four experiments in the regime of double resonance, when the decoupler frequency was between the positions of the ReH lines followed by an averaging of the $A(0)$ values. The intensities $A(S)$ were taken from three to four experiments in the regime of double resonance when one of the ReH signals was saturated by the use of the decoupler operating in the CW or pulse mode. The application of $^1$H routine decoupling powers turned out to be sufficient to achieve a maximum saturation transfer. The inversion recovery method (180°−$\tau$−90°) was used to determine $T_1$(ReH) relaxation times. The calculations of the relaxation times were performed using a nonlinear three-parameter fitting routine of the spectrometer. The $T_1$ values for the ReH nuclei were found to be practically identical for both diastereomeric H ligands of **1**−**4**;[11] however, they were strongly differing within the series of these compounds: the smallest values were found for **1** ($T_1$(ReH) = 0.26 s at 16 °C), and the largest values were determined for **2** ($T_1$(ReH) = 3.3 s at 16 °C).

The ReH$_2$(CO)(NO)L$_2$ compounds **1**−**4** were prepared as described in the literature.[10] The concentrations used in the NMR experiments were approximately 0.15 mol/L. Isotopic mixtures of ReH$_2$(CO)(NO)L$_2$, ReHD(CO)(NO)L$_2$, and ReD$_2$(CO)(NO)L$_2$ suitable for the kinetic isotope effect measurements were prepared from the corresponding ReH$_2$ complexes (dissolved in toluene-$d_8$) by H/D echange with CD$_3$OD at 50 °C as described in an earlier paper.[15] The H/D exchanges were monitored by $^1$H NMR and the solvent mixtures were evaporated in *vacuo* after completion of the reaction. $^1$H NMR for ReHD(CO)(NO)L$_2$: L = PCy$_3$ (**1**; toluene-$d_8$/CD$_3$OD, 40 °C), H$_b$ −1.30 ppm ($J$(P−H) = 26.3 Hz), H$_a$ −5.10 ppm ($J$(P−H) = 24.0 Hz); L = P(OiPr)$_3$ (**4**; toluene-$d_8$/CD$_3$OD, 25 °C) H$_b$ −2.07 ppm ($J$(P−H) = 29.5 Hz), H$_a$ −5.26 ppm ($J$(P−H) = 31.9 Hz). The $J$(H−D) coupling could not be resolved.

The calculations were performed using the MEHT[21] and CACAO[23] program packages. The parameters for Re were as follows: 5d, $H_{ii}$ = −12.66 eV, $\zeta_1$ = 5.343, $\zeta_2$ = 2.277, $c^1$ = 0.6359, $c^2$ = 0.5677; 6s, $H_{ii}$ = −9.36 eV, $\zeta$ = 2.398; 6p, $H_{ii}$ = −5.96 eV, $\zeta$ = 2.372. Those for the other atoms were the standard values of CACAO. The following distances (Å) were used in all computational procedures: Re−CO, 1.92; Re−NO, 1.80; Re−PH$_3$, 2.43; C−O, 1.08; P−H, 1.40. The angular degrees of freedom chosen to simulate a tetrahedral-jump rearrangement of **5** along paths **A** and **B** (see Table 4).

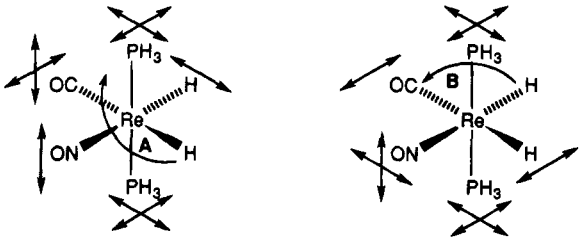


**Acknowledgment.** Financial support from the Swiss National Science Foundation is gratefully acknowledged.

OM9402170

(23) Mealli, C.; Proserpio, D. M. *J. Chem. Educ.* **1990**, *67*, 399.